ORIGINAL ARTICLE

Influence stacking sequence and heat treatments on the out-of-plane mechanical properties of 3D-printed fiberglass-reinforced thermoplastics

Rodolfo Hermosilla[1] · Angelo Oñate[2,3] · Rodrigo Castillo[3] · Andrés De la fuente[1] · Joaquín Sepúlveda[1] · Benjamín Escudero[1] · Gustavo Vargas-Silva[4] · Víctor Tuninetti[5] · Manuel Melendrez[2] · Carlos Medina[1,6]

Abstract

Additive manufacturing of composite materials is a promising technology. It could solve one of the most critical drawbacks of 3D-printed fiber-reinforced thermoplastics: their low out-of-plane mechanical properties. Due to this factor, it is still unknown how most design and manufacturing parameters affect the out-of-plane properties of composite materials. As a solution, this paper proposes an experimental methodology to characterize out-of-plane printed composite materials. For this purpose, existing standards for traditionally fabricated composites are adapted, investigated, and validated for 3D-printed laminates reinforced with long fibers using the fused filament fabrication technique. Consequently, the methodology is employed to study the impact of stacking sequence and heat treatment conditions on the composites' out-of-plane mechanical properties. The main results showed that increasing the thickness between stacking layers increases the mechanical response due to reducing the number of fiber/matrix interfaces and, consequently, the reduction of porosity. Compared to the initial sample, a heat treatment at 175 °C for 6 h increased the interfacial strength by 101.09% and reduced the porosity in the fiber produced by the additive manufacturing process by 72%.

Keywords Fused filament fabrication · Interlaminar strength · Stacking sequences · Void reduction

✉ Angelo Oñate
aonates@udec.cl

✉ Carlos Medina
cmedinam@udec.cl

1 Department of Mechanical Engineering (DIM), Faculty of Engineering, Universidad de Concepción, Edmundo Larenas 219, Concepción, Chile

2 Department of Materials Engineering (DIMAT), Faculty of Engineering, Universidad de Concepción, Edmundo Larenas 270, Concepción, Chile

3 Department of Mechanical Engineering (DIMEC), Faculty of Engineering, Universidad del Bío – Bío, Av. Collao 1202, Concepción, Chile

4 Engineering Department, Public University of Navarre (UPNA), Campus of Arrosadia, 31006 Pamplona, Spain

5 Department of Mechanical Engineering, Universidad de La Frontera, Francisco Salazar 01145, 4780000 Temuco, Chile

6 Centro para Industria 4.0 – C4i, Universidad de Concepción, Edmundo Larenas 219, Concepción, Chile

1 Introduction

Even though the benefits of 3D printing have been widely documented, there still remain some critical challenges to overcome in order to make the technology viable to fabricate thermoplastic industrial end products, such as increasing its repeatability and dimensional accuracy [1], and the relatively low mechanical properties when compared with those manufactured by traditional fabrication techniques [2, 3].

A recent solution has been to reinforce thermoplastic printed components with stiffening and strengthening elements like short fibers [4–6], long fibers [7–9], and particles [10, 11], or in other words, to 3D print fiber-reinforced composite materials. 3D-printed composites extend the capabilities of traditional composites, as they can be easily manufactured with complex geometries [12–14]. However, compared with traditionally fabricated parts [15–17], they still exhibit a notably lower mechanical performance as the thermomechanical nature of AM processes negatively impacts the resulting microstructure and, consequently, their behavior. For example, 3D-printed composites present more

internal voids and discontinuities than their counterparts, which facilitates the propagation of transverse cracks and degrades the bonds between their constitutive elements [18, 19]. Some approaches to correct this issue include compacting forces on the printing process through external devices like compression molds [18] and compaction rollers [20, 21]. These investigations have also confirmed the strong correlation between void content and mechanical performance, as void reduction has produced proportional improvements in mechanical properties. Other drawbacks of printed composites are poor interlaminar adhesion caused by the premature cooling of in-bed layers before the following layer is deposited [22, 23], low fiber volume fractions due to limitations of the process, and difficulty in the extrusion of denser fiber bundles through the nozzle [24].

These negative impacts cannot be avoided but can be dampened by adjusting the printing parameters. For example, Rimasauskas et al. [25] analyzed the dependency of tensile properties of carbon fiber-reinforced polylactide acid (PLA) on layer height and line width by comparing the mechanical properties, void percentage, and fiber content. They concluded that manufacturing parameters greatly affect the features of the resulting microstructure, mainly the void content and the fiber volume fraction, modifying mechanical performance. Other investigations addressing the impact of printing configuration on mechanical properties include the effects of nozzle geometry [26, 27], reinforcement type [28, 29], printing speed [27], printing temperature [30], and stacking sequence [31]. Chacón et al. [29] studied the influence of fiber volume content on tensile and flexural properties of 3D-printed specimens by varying the number of fiber layers at the cross-section, noting that increasing the number of fiber plies both increases stiffness and strength and rises the number of microstructural defects. Shi et al. [32] compared the tensile properties of three reinforcement distributions: concentrated, halve, and quartering. The mechanical constants varied for each arrangement, with the quartering sequences showing the highest tensile modulus and the halving sequences the highest stiffness. Nevertheless, most of these investigations have addressed the repercussions of printing configuration on the in-plane directions, with few exceptions focused on the out-of-plane response, and usually covering the impact of a limited number of parameters on the flexural stiffness and strength [29, 33] and the interlaminar behavior [34].

In part, this scarcity is caused by the absence of investigations aiming to develop new methods or exploring the feasibility of existing methods and standards usually employed for traditional composites, to identify the out-of-plane mechanical constants of printed materials. Hence, an experimental methodology to characterize the out-of-plane mechanical behavior of 3D-printed composite materials under tensile, compression, and interlaminar shear loading is proposed. The procedures consist in adaptations of the ASTM D7291/D7291M [35], ASTM D695-15 [36], and the ASTM D2344/D2344M [37] standards, complemented with previous works addressing the out-of-plane characterization of traditionally fabricated composites. Afterwards, the proposed methodology is employed to study the influence of the number of stacked plies on the tensile elastic modulus (E_{33}^{tr}), the ultimate tensile strength ($\sigma_{33,u}^{tr}$), the compressive elastic modulus (E_{33}^{com}), the compressive yield strength ($\sigma_{33,0}^{com}$), the ultimate compressive strength ($\sigma_{33,u}^{com}$), and the interlaminar shear strength (τ_{ILSS}). For this purpose, mentioned mechanical properties of three stacking configurations are compared: 1 fiber–1 matrix–1 fiber (1O1F), 2 fiber–2 matrix–2 fiber (2O2F), and 3 fiber–3 matrix–3 fiber (3O3F), with all specimens made of fiberglass-reinforced onyx printed by the fused filament fabrication (FFF) technique. Then, the results are compared with those present in the literature.

A technique that has been effective in enhancing the mechanical properties of 3D-printed composites is the use of heat treatments (HT) once fabricated. Microscopical observations have demonstrated that as the polymeric matrix is heated over its crystallization point, its microstructure progressively rearranges, causing a decrease of its discontinuities and an improvement of its interlayer bonds and crystallization [33, 38, 39]. Analogously to the repercussions of fiber distribution, the effects of HT in the out-of-plane mechanical constants have been vaguely studied for printed laminates. To the best of the author's knowledge, the only published research work on this matter is the work of Wang et al. [33] consistent in determining how heat treatment conditions affect the crystallization, porosity, and flexural and tensile properties of laminates, continuously and separately reinforced with UD-fiber plies. Consequently, the proposed methodology is employed to study the influence of HT conditions on the laminate's τ_{ILSS}. With that in mind, a set of 3O3F specimens are heat-treated at 100 °C, 150 °C, and 175 °C for 6 h. Then, the treated specimens are characterized in terms of τ_{ILSS}, mass, size, and void percentage, with the latter being especially important as several authors point it out as a determinant factor to the mechanical performance, as previously explained. Based on these results, the relation between HT conditions and interlaminar shear strength is discussed and contrasted with the results available in the literature.

2 Methodology

2.1 Experimental setup

The coupons are fabricated using a Markforged Mark Two printer, capable of printing continuously reinforced thermoplastics using the fused filament fabrication (FFF) method.

This machine can fabricate up to $320 \times 132 \times 154$ mm parts with a 100 to 200 μm layer thickness by depositing material through two independent nozzles: one for thermoplastic matrix, and another for fiber bundles. The materials used to fabricate the specimens are ONYX® and HSHT® fiberglass continuous filament developed by Markforged [40] (see Fig. 1). The mechanical properties are shown in Table 1.

Tensile mechanical characterization and flexure was performed on a ZwickRoell Z005 universal testing machine with a load capacity of 5 kN at a strain rate of 1 mm/min. The compression test was performed on an Instron 8801 universal testing machine with a 100 kN load cell at a loading rate of 1 mm/min. An RS PRO 120 Ω extensometer connected to a Micro-Measurements P3 strain gauge system was used to assist testing requirements.

Heat treatments (HT) were performed on an SZGL-1200C vacuum tube furnace with a heating ramp of 15 °C/min and air natural cooling, and the temperatures used were 100 °C, 150 °C, and 175 °C. Heat treatments were applied for 6 h only to the stacking sample that obtained the best mechanical response, similar as Wang et al. [33] and Pascual-Gonzalez et al. [41].

To analyze the reduction in porosity, heat-treated samples were cross-sectioned and sanded with SiC sandpaper mesh size between 240 and 2400, and polished on a polishing table with 0.05 μm alumina suspension. The cross-section of the samples was characterized to quantify porosity using a Leica DMi8 microscope with a magnification of $200 \times$. Images were then processed using ImageJ software to quantify porosities. Porosities were quantified by particle analysis, calibrating the image, and transforming it to 8 bits to adjust the porosity threshold. Furthermore, the density was measured by the Archimedean principle using a Radwag AS 220/C/2 precision analytical balance.

2.2 Stacking sequences

Figure 2 outlines the characterized reinforcement distributions, where F and O stand for fiber- and onyx-section. All continuous fibers were printed with a 0° orientation as tensile and flexural properties are maximized at this fiber angle [42]. Subsequently, the XOYF notation will be employed to designate the reinforcement configurations, where X represents the number of intermediate onyx layers and Y the number of continuous fiber plies above and below them, with 0.1 mm thickness each.

Three samples were fabricated for each test of each reinforcement distribution to ensure statistical representativeness. Even though standards such as ASTM D7291/D7291M suggest employing at least five specimens, it points out that valid results can be obtained using fewer specimens. As for the HTs, two specimens were subjected to each treatment configuration and subsequently characterized.

2.3 Out-of-plane compression test

Up to now, no standard has been developed for compression mechanical testing of 3D-printed composites. In this paper, the methodology proposed by Kim et al. [43] based on the ASTM D695 standard was adopted. As opposed to Kim, who cut the specimens from a laminate using a wheel cutter, the specimens depicted in Fig. 3 were printed ready to be tested. Analogously to tensile properties ("Sect. 2.4"), elastic compressive modulus E_{33}^{com} and ultimate compressive

Fig. 1 Schematic diagram of the 3D printing process of composite materials produced by fused filament fabrication
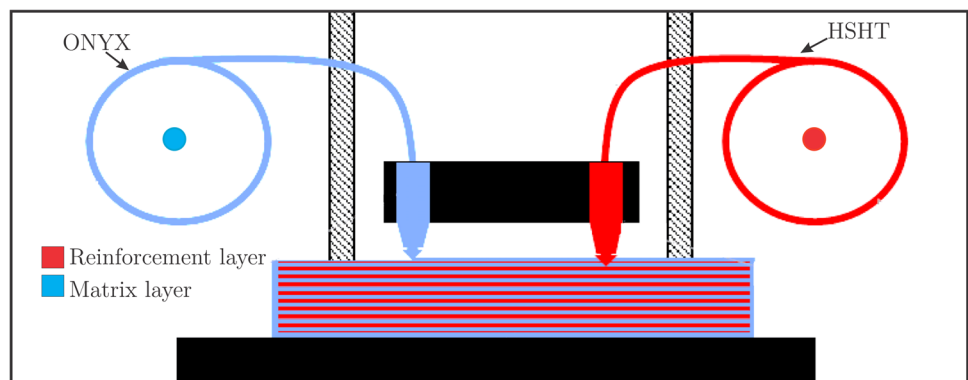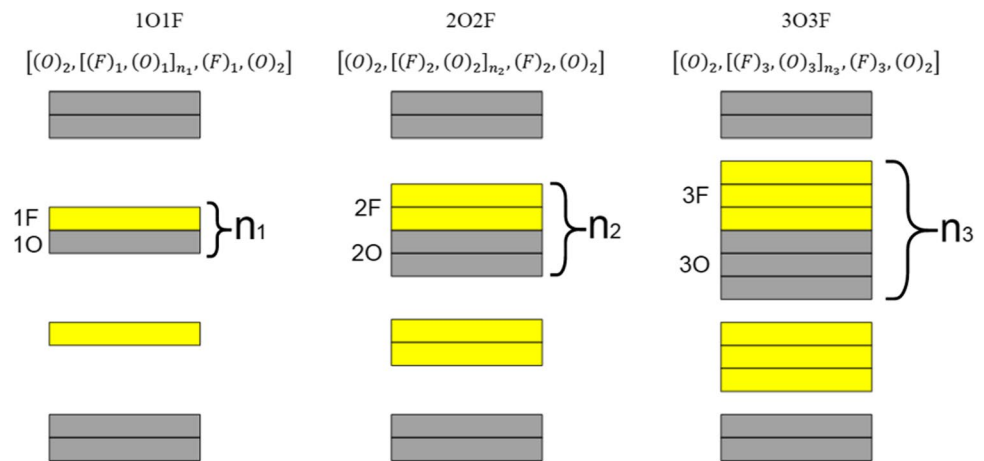
Table 1 Mechanical properties of the specimens' constitutive materials [40]

Material	Tensile modulus GPa	Tensile strength MPa	Compressive modulus GPa	Compressive strength MPa	Flexural modulus GPa	Flexural strength MPa
Onyx	2.4	37	–	–	3	71
HSHT fiberglass	21	600	21	216	21	420

Fig. 2 Characterized stacking sequences

Fig. 3 Out-of-plane compressive mechanical testing
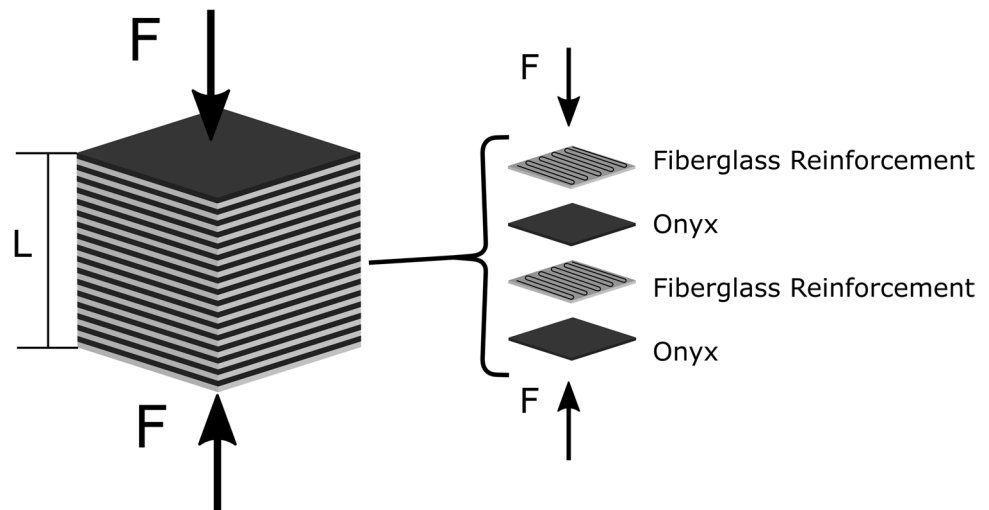
strength $\sigma_{33,u}^{com}$ correspond to the slope of the elastic region and the stress at failure in the stress–strain curve, respectively. Compressive yield strength $\sigma_{33,0}^{com}$ is estimated as the value of stress where the relationship between σ and ε is no longer linear.

2.4 Out-of-plane tensile test

The monotonic tensile tests were carried out based on recommendations by San Juan et al. [44] and the ASTM D7291/7291 M standard. Accordingly, the specimens were designed with the spool configuration and the load acting as illustrated in Fig. 4. At first, the tabs were made of steel and attached to the specimens through a fast-action epoxy adhesive, as suggested by San Juan et al. [44]. However, most tests were unsuccessful as the adhesive interface between the tab and the specimen failed prematurely due to a weak bond between the adhesive and the onyx matrix. This issue was corrected by taking advantage of feature of 3D printing mentioned: its capacity to print complex geometries by including

the tabs directly in the CAD model. Nonetheless, as onyx-matrix tabs are quite flexible, the strain measured with the machine's extensometer is not representative. Hence, out-of-plane strain was measured by allocating a strain gauge on the laminate to guarantee that measured deformation only corresponds to the reinforced section.

The two-layer coating added by the printer is removed on a lathe through a 2 mm diameter reduction. As exemplified in Fig. 5, the extracted material adds up to 50% of the original transverse area, potentially interfering with the laminate's response.

From measured stress–strain response, the out-of-plane tensile elastic modulus E_{33}^{tr} corresponds to the slope of the elastic region of the curve, and the ultimate tensile strength $\sigma_{33,u}^{tr}$ is equal to the stress at failure.

2.5 Interlaminar shear strength (ILSS) test

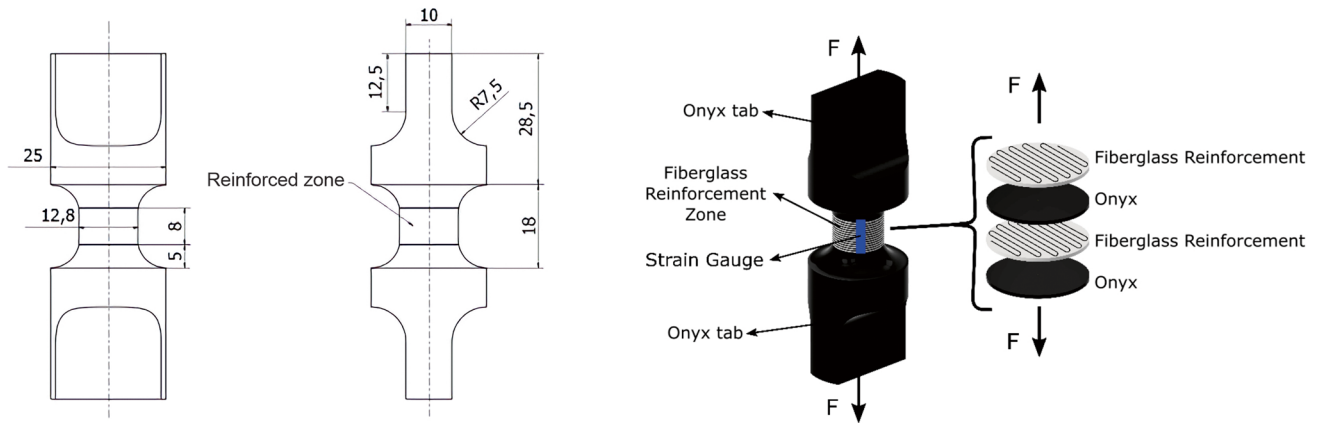The ASTM D2344/D2344M standard was used to obtain the interlaminar shear strength, adopting the 3-point bending test

Fig. 4 Out-of-plane tensile mechanical testing

on a short beam shear (SBS). The specimen dimensions are a function of the thickness $t = 5.9$ mm for all stacking sequences (see Fig. 6). The nose and the supports are free of indentations and burrs that allow lateral displacement of the specimen, reducing additional stresses that generate non-representative results. The schematic detail of the test is shown in Fig. 6. The load is applied with a speed of 1 mm/min monotonically until a load drop of 30% is reached, the specimen fails, or the head travel exceeds the nominal thickness of the specimen.

According to mentioned standard, the ILSS of the laminate is calculated as follows:

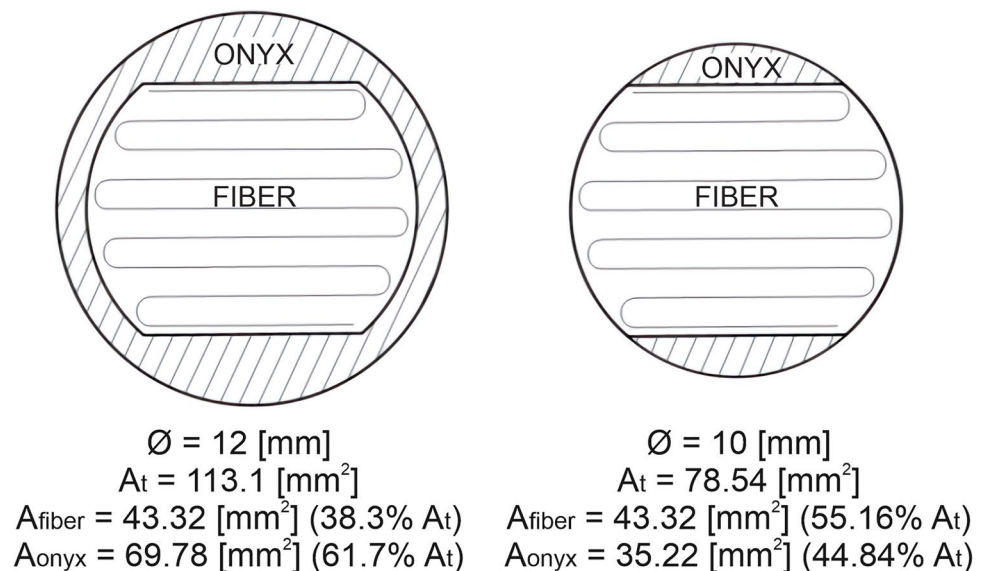$$\tau_{ILSS} = \frac{3P_{max}}{4\ bt} \tag{1}$$

where P_{max} is the value of the load at failure, b is the laminate width, and t is its height.

3 Results and discussions

3.1 Reinforcement distribution

The results of the compressive tests are shown in Fig. 7. Because of the similarities in the measured response of specimens for each stacking sequence, the mean stress–strain curves of 1O1F, 2O2F, and 3O3F laminates are presented. Mean curves were estimated as the interpolation of the experimental data of each test in terms of a normalized strain array and the subsequent point-by-point averaging of stress values. It is evident that out-of-plane compression behavior exhibits almost complete independence from the number of stacked plies, as its variation produces nearly insignificant changes in compressive stiffness and ultimate compressive strength, as detailed in Table 2. All failed specimens

Fig. 5 Cross-section of the tensile specimens before and after a 2 mm diameter reduction in a lathe
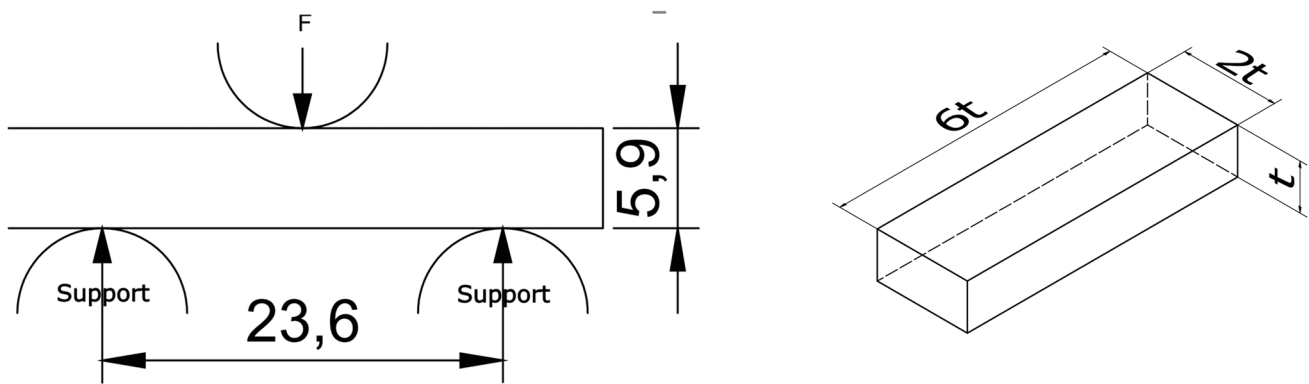

Ø = 12 [mm]
At = 113.1 [mm^2]
Afiber = 43.32 [mm^2] (38.3% At)
Aonyx = 69.78 [mm^2] (61.7% At)

Ø = 10 [mm]
At = 78.54 [mm^2]
Afiber = 43.32 [mm^2] (55.16% At)
Aonyx = 35.22 [mm^2] (44.84% At)

Fig. 6 Characteristics of the three-point bending short beam shear test performed to identify the laminate interlaminar shear strength

Fig. 7 Out-of-plane stress–strain response of the monotonic compressive tests for all reinforcement distributions
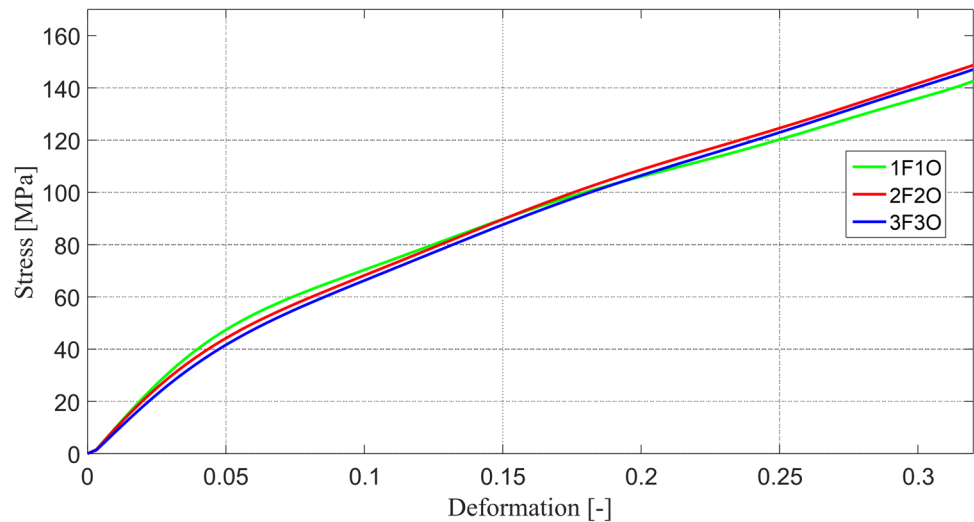
presented multiple transverse cracks demonstrating that the laminate's failure occurs as the matrix collapses when it cannot support the compressive load any longer. The augmentation of the plies' thickness seems only to affect the length of these cracks but does not influence their propagation, resulting in an almost identical behavior for all the stacking arrangements.

Figure 8 shows the stress–strain response obtained for the out-of-plane monotonic tensile tests. The increase in the number of plies results in an increase in the ultimate tensile strength of the laminate due to a reduction in the number of fiber/onyx interfaces, with the 1O1F samples being the least strong and the 3O3F being the strongest. An inverse relation exists regarding the material's stiffness, with its progressive decrease for a higher number of plies. This effect is attributed to porosity effects at the fiber/onyx interface caused by the FFF printing method. Studies such as Ning et al. [8] corroborate the effect of porosity on mechanical response in thermoplastic composites made by additive manufacturing, showing that increased porosity at the interface reduces the tensile mechanical response. However, reinforcement distribution also influences ductility, with 3O3F elements

Table 2 Identified out-of-plane mechanical properties for different stacking sequences of fiberglass-reinforced onyx

Stacking sequence	Tension		Compression			SBS
	Elastic modulus GPa	Strength MPa	Elastic modulus GPa	Yield strength MPa	Strength MPa	Strength MPa
1O1F	4.48	7.34	1.19	44.58	142.4	15.81
2O2F	3.2	8.32	1.14	38.77	148.8	16.04
3O3F	2.53	8.97	1.02	38.36	147.2	19.27

Fig. 8 Out-of-plane stress–strain response of the monotonic tensile tests for all reinforcement distributions
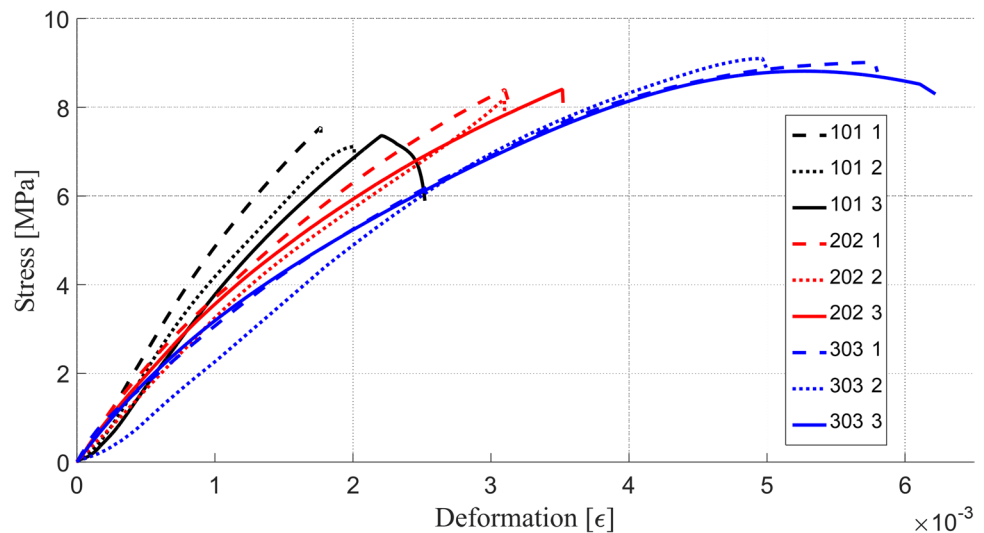

reaching approximately three times the 1O1F coupons strain at failure. Another significant observation at this point is that specimens presented different failure modes. For 1O1F and 2O2F sequences, when ultimate tensile strength is reached, the laminates present a fragile rupture characterized by an abrupt drop in stress. Furthermore, for 3O3F sequences, this transition is smoother even after failure evidencing a ductile behavior.

Figure 9 presents the measured flexural mechanical behavior for all coupons tested by short beam shear. Analogous to the out-of-plane tensile tests in Fig. 8, the increase in the number of plies results in vertical displacement of the stress–strain curve, especially after the onset of creep. Consequently, the average interlaminar shear strength of the 3O3F laminate is 22% higher than the τ_{ILSS} of the 1O1F stacking sequence, as shown in Table 2. The increased porosity causes the above in laminates with

a higher number of fibers/onyx interface. This porosity decreases the interfacial strength due to the increased stress inducing damage. Two failure modes occurred regardless of the reinforcement distribution, i.e., both were present for each stacking configuration. The first is interlaminar delamination from the ends of the specimen (see Fig. 10c), causing a brittle failure noticeable in the τ_{ILSS} vs δ response of the material (see Fig. 9) through the sharp decrease in strain once the interlaminar shear strength is exceeded. The second type is delamination splitting consecutive interlaminar (see Fig. 10d), reducing the damage rate, and causing a ductile failure characterized by a smooth stress transition after τ_{ILSS}.

Figure 10 shows the types of failures obtained for each test. The tensile samples represented in Fig. 10a failed at the fiber/matrix interface induced by the effect of porosity. Figure 10b represents the samples tested at 1O1F compression.

Fig. 9 Flexural stress-displacement response of the three-point bending short beam shear test for all reinforcement distributions
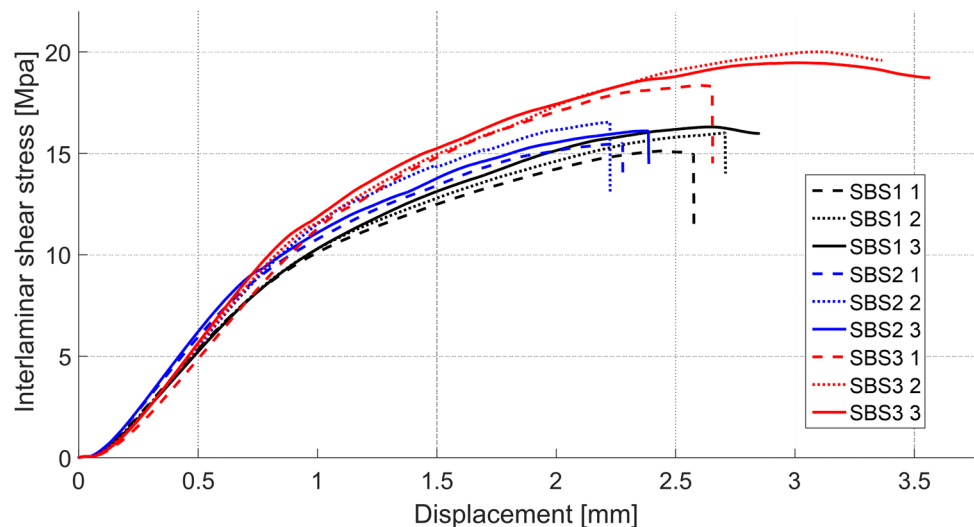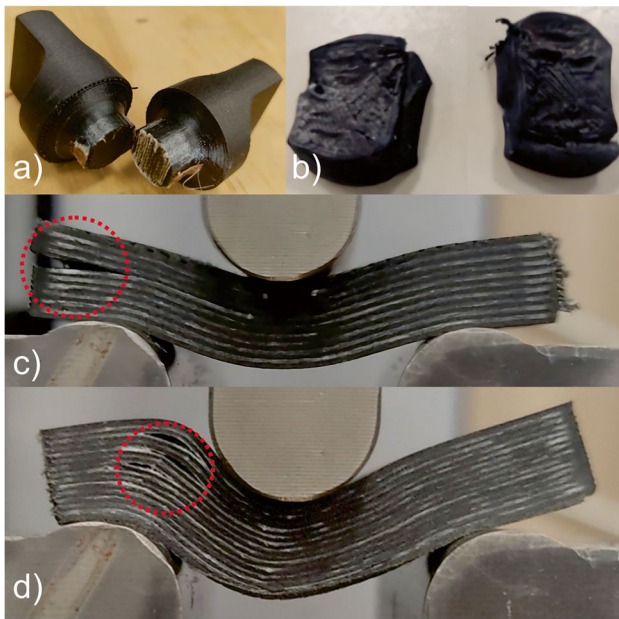
Fig. 10 Representative failed specimens of the different stacking sequences: **a** traction; **b** compression 101F; **c** shear debonding; **d** shear delamination

Figure 10c and d represent the specimens tested in 3-point bending SBS, indicating the types of failure indicated above, which consist of delamination from the edge of the specimen causing severe damage causing brittle failure (see Fig. 10c) and delamination in multiple internal layers (see Fig. 10d), which causes a significant reduction in the damage rate by increasing the energy absorption between the interlaminar layers producing a ductile failure.
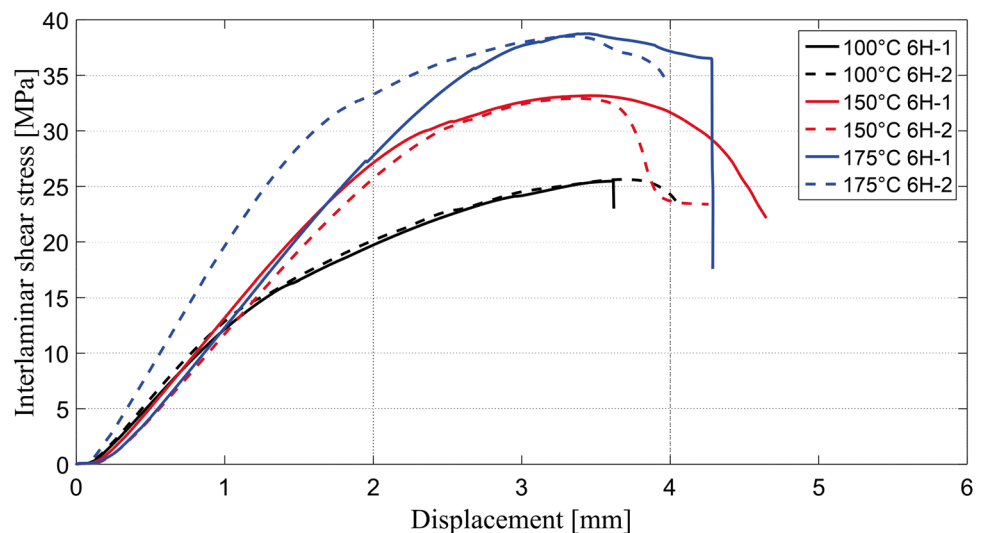
3.2 Heat treatment

For the sake of simplicity, only the HTs that caused the most significant improvements of the mechanical properties are analyzed. Figure 11 shows the τ vs. δ response of the 3O3F treated specimens. While stiffness seems unaffected by the HT, except for the 175 °C 6H-1 configuration, it is clear the existence of a strong dependency of τ_{ILSS} and plasticity evolution on the HT conditions, with the enhancement of the mechanical properties as temperature and duration increase. Consistently, better performance is achieved by the 175 °C 6H treatments with almost two times the τ_{ILSS} exhibited by the untreated specimens of identical stacking configuration.

As detailed in Table 3, a correctly designed heat treatment is more effective in enhancing the interlaminar properties of the laminate than augmenting its number of plies, whether of fiber or matrix. For example, untreated 3O3F laminates reached a 32.16% superior τ_{ILSS} than untreated 1O1F laminates (from 15.14 to 20.01 MPa), while 175 °C 6H 3O3F laminates achieved a 93.65% improvement vs. untreated 3O3F sequences (from 20.01 to 38.75 MPa). With the combination of both factors, i.e., an increase in the number of

Table 3 Summary of the heat treatment conditions that achieved the most significant improvement of τ_{ILSS}

Stacking sequence	Heat treatment		τ_{ILSS} MPa
	Temperature °C	Duration h	
303F	–	–	20.01
303F	100	6	25.62
303F	150	6	33.17
303F	175	6	38.75

Fig. 11 Flexural stress-displacement response of the three-point bending tests performed in heat-treated specimens

stacked plies and subsequent heat treatment, an improvement of 155.94% in τ_{ILSS} is achieved (from 15.14 to 38.75 MPa).

As mentioned in "Sects. 1 and 3.1," the porosities obtained by additive manufacturing processes of composites negatively affect the mechanical response of the material [18]. The heat-treated samples increased interlaminar adhesion, which is attributed to a reduction of porosities at the fiber/onyx interface due to an entanglement effect of the reinforcement and matrix at the points of lower interfacial energy (porosities) resulting from molecular activation and diffusion. This entanglement effect between the fiber and the onyx reduces the pores because they cover the voids at the interface, improving their interfacial mechanical response. Additionally, there is an increase in the crystallinity of the composite, increasing the interfacial binding energy.

The result of porosity reduction obtained by optical microscopy analysis and image processing in ImageJ software are represented in Table 4. It is possible to observe that two types of porosities were found, which were classified as fiber porosity and matrix porosity. The porosity in the

matrix is mainly due to the preparation of the sample by tearing off the short fiber reinforcement with sanding and subsequent polishing. The above shows a porosity rate without significant variation in the heat-treated and non-heat-treated samples, respectively. However, the porosity in the fiber directly affects the interfacial strength because it interacts with the fiber/matrix interface, and the voids are significantly reduced with heat treatment (see Fig. 12). Based on the results obtained from the heat treatment, it is deduced that the interfacial strength is strongly related to the porosity produced in the fiber during the additive manufacturing process by the fused filament fabrication (FFF) method.

The relationship between temperature and the reduction of porosity in the fiber is attributed to molecular activity; therefore, the higher the temperature, the more intense the molecular activity is, and the more porosity is reduced by increasing the diffusion of entanglement between the fiber and the matrix. Figure 12 shows the morphology and effect of heat treatment on porosity at 200 × magnification. Figure 12a shows sample 303 without heat treatment and with the characteristic porosity in the fiber. As the heat treatment is increased, it is observed how the effect of entanglement covers the porosity. For the temperature of 100 °C, it is observed that the molecular activation energy is low, so the porosity is not entirely covered, resulting in an insignificant change in the interfacial resistance (see Table 3). In contrast, for samples heat treated at 150 °C and 175 °C, complete entanglement and a reduction in porosity size are observed. The increase in interfacial strength with the reduction in

Table 4 Void percentage variation for 6 h of heat treatment at 100 °C, 150 °C, and 175 °C

Temperature	Without HT	100 °C	150 °C	175 °C
Porosity in matrix	10.73%	10.42%	9.62%	8.28%
Porosity in fiber	6.58%	4.11%	2.90%	1.83%
Total porosity	17.31%	14.53%	12.52%	10.11%

Fig. 12 Porosity in mechanically characterized 303 samples: **a** sample without heat treatment; **b** sample with heat treatment at 100 °C for 6 h; **c** sample with heat treatment at 150 °C for 6 h; **d** sample with heat treatment at 175 °C for 6 h
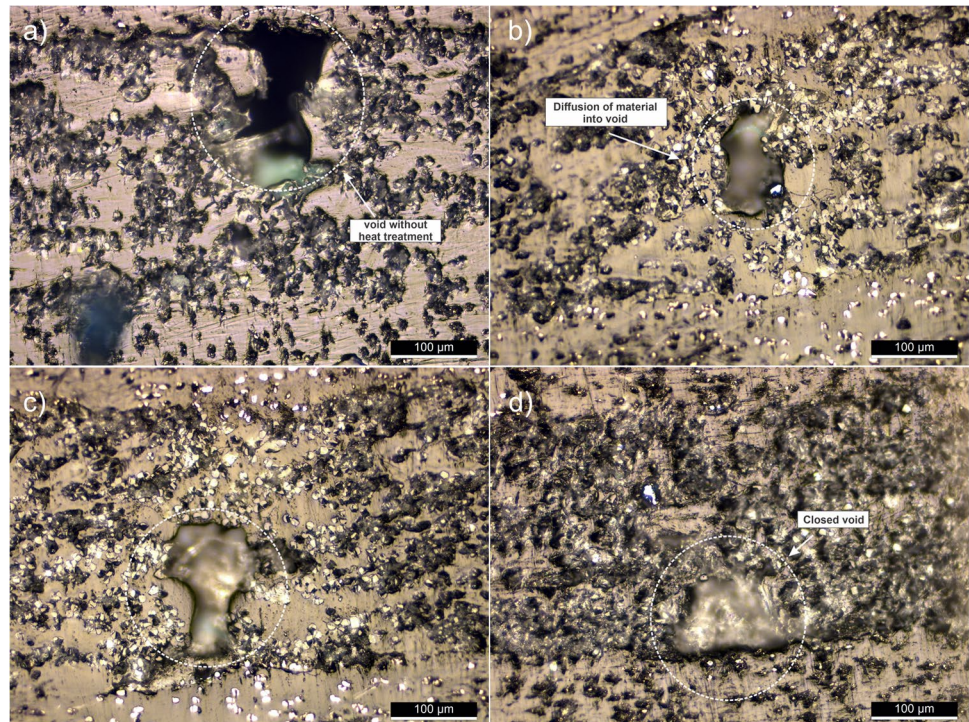
thickness obtained in this study is consistent with results obtained by Hart et al. [45, 46], thus validating our findings. The density results indicated that the density increased with an increase in heat treatment temperature. This increase in density is attributed to the reduction of porosity while keeping the volume constant, which corresponds with the optical microscopy results observed in Table 4 and Fig. 12.

4 Conclusion

The effect of stacking configuration on the mechanical response of the composite and the effect of heat treatment on the interfacial mechanical strength and porosity reduction were studied separately. The main drawback observed is that the manufacturing process produces a high amount of porosity, which influences the mechanical response. However, a temperature range has been found that improves the interfacial response in this type of materials fabricated by FFF, which could significantly favor industrial applications and reduce the mechanical problems that these materials usually present. In addition, its high capacity for parameterized fabrication allows for obtaining complex parts and manufacturing laminated composites with an optimized mechanical response. The samples in the temperature range studied do not present a significant dimensional change, indicating high feasibility as post-processing in parts requires rigorous dimensional tolerance. The results showed that:

- The increase in fiber and matrix thickness of the stack improves the mechanical response of the composite material by reducing the amount of porosity produced by the FFF manufacturing process and increasing the contribution of matrix ductility.
- The out-of-plane compression test is unsuitable for measuring interlaminar behavior due to the failure mode.
- The heat treatment generating the best interlaminar response was 175 °C for 6 h. This best response is attributed to the higher molecular activation for mobility and entanglement effect on fiber and matrix porosity. The results indicated a 101.09% increase in interlaminar strength and a 72% reduction in fiber porosities over the 303 laminates without heat treatment.

Declarations

References

1. Dowling L, Kennedy J, O'Shaughnessy S, Trimble D (2020) A review of critical repeatability and reproducibility issues in powder bed fusion. Mater Des 186:108346. https://doi.org/10.1016/J.MATDES.2019.108346

2. Kabir SMF, Mathur K, Seyam AFM (2020) A critical review on 3D printed continuous fiber-reinforced composites: history, mechanism, materials and properties. Compos Struct 232:111476. https://doi.org/10.1016/J.COMPSTRUCT.2019.111476

3. Chapiro M (2016) Current achievements and future outlook for composites in 3D printing. Reinf Plast 60:372–375. https://doi.org/10.1016/J.REPL.2016.10.002

4. Zhong W, Li F, Zhang Z, Song L, Li Z (2001) Short fiber reinforced composites for fused deposition modeling. Mater Sci Eng, A 301:125–130. https://doi.org/10.1016/S0921-5093(00)01810-4

5. Zak G, Haberer M, Park CB, Benhabib B (2000) Mechanical properties of short-fibre layered composites: prediction and experiment. Rapid Prototyp J 6:107–118. https://doi.org/10.1108/13552540010323583/FULL/XML

6. Kruth JP, Levy G, Klocke F, Childs THC (2007) Consolidation phenomena in laser and powder-bed based layered manufacturing. CIRP Ann 56:730–759. https://doi.org/10.1016/J.CIRP.2007.10.004

7. Masaki Namiki, Masahito Ueda, Akira Todoroki, Yoshiyasu Hirano, Ryosuke Matsuzaki (2014) 3D Printing of Continuous Fiber Reinforced Plastic. In Proceedingsof the SAMPE Tech Seattle 2014 Conference SAMPE, p 1–6. https://www.nasampe.org/store/ViewProduct.aspx?ID=4415595.

8. Ning F, Cong W, Qiu J, Wei J, Wang S (2015) Additive manufacturing of carbon fiber reinforced thermoplastic composites using fused deposition modeling. Compos B Eng 80:369–378. https://doi.org/10.1016/J.COMPOSITESB.2015.06.013

9. De-Vivo L (2017) Design and manufacture of optimized continuous composite fiber filament using additive manufacturing systems. J Mater Sci Eng 6:363. https://doi.org/10.4172/2169-0022.1000363

10. Kalsoom U, Nesterenko PN, Paull B (2016) Recent developments in 3D printable composite materials. RSC Adv 6:60355–60371. https://doi.org/10.1039/C6RA11334F

11. Ngo TD, Kashani A, Imbalzano G, Nguyen KTQ, Hui D (2018) Additive manufacturing (3D printing): a review of materials, methods, applications and challenges. Compos B Eng 143:172–196. https://doi.org/10.1016/J.COMPOSITESB.2018.02.012

12. Patel A, Taufik M (2022) Stage dependent strengthening of fused filament fabricated components. Mater Today Proc 50:1853–1861. https://doi.org/10.1016/J.MATPR.2021.09.231

13. Holmes M (2019) Additive manufacturing continues composites market growth. Reinf Plast 63:296–301. https://doi.org/10.1016/J. REPL.2018.12.070

14. Dizon JRC, Espera AH, Chen Q, Advincula RC (2018) Mechanical characterization of 3D-printed polymers. Addit Manuf 20:44–67. https://doi.org/10.1016/J.ADDMA.2017.12.002

15 Muskeri S, Hasannaeimi V, Salloom R, Sadeghilaridjani M, Mukherjee S (2020) Small-scale mechanical behavior of a eutectic high entropy alloy. Sci Rep 10:1–12. https://doi.org/10.1038/s41598-020-59513-2

16. Cao D, Malakooti S, Kulkarni VN, Ren Y, Liu Y, Nie X, Qian D, Griffith DT, Lu H (2022) The effect of resin uptake on the flexural properties of compression molded sandwich composites. Wind Energy 25:71–93. https://doi.org/10.1002/WE.2661

17. Wang X, Xu T, de Andrade MJ, Rampalli I, Cao D, Haque M, Roy S, Baughman RH, Lu H (2021) The interfacial shear strength of carbon nanotube sheet modified carbon fiber composites. Conf Proc SocExp Mech Ser 25–32. https://doi.org/10.1007/978-3-030-59542-5_4

18. He Q, Wang H, Fu K, Ye L (2020) 3D printed continuous CF/PA6 composites: effect of microscopic voids on mechanical performance. Compos Sci Technol 191:108077. https://doi.org/10.1016/J.COMPSCITECH.2020.108077

19. Yang D, Zhang H, Wu J, McCarthy ED (2021) Fibre flow and void formation in 3D printing of short-fibre reinforced thermoplastic composites: an experimental benchmark exercise. Addit Manuf. 37:101686. https://doi.org/10.1016/J.ADDMA.2020.101686

20. Ravoori D, Salvi S, Prajapati H, Qasaimeh M, Adnan A, Jain A (2021) Void reduction in fused filament fabrication (FFF) through in situ nozzle-integrated compression rolling of deposited filaments. Virtual and Physical Prototyping 16:146–159. https://doi.org/10.1080/17452759.2021.1890986

21. Omuro R, Ueda M, Matsuzaki R, Todoroki A, Hirano Y (2017) Three-dimensional printing of continuous carbon fiber reinforced thermoplastics by in-nozzle impregnation with compaction roller. In Proceedings of the 21st International Conference on Composite Materials 21:343–354. https://iccm-central.org/Proceedings/ICCM21proceedings/papers/4639.pdf

22. Kishore V, Ajinjeru C, Nycz A, Post B, Lindahl J, Kunc V, Duty C (2017) Infrared preheating to improve interlayer strength of big area additive manufacturing (BAAM) components. Addit Manuf 14:7–12. https://doi.org/10.1016/J.ADDMA.2016.11.008

23. Justo J, Távara L, García-Guzmán L, París F (2018) Characterization of 3D printed long fibre reinforced composites. Compos Struct 185:537–548. https://doi.org/10.1016/J.COMPSTRUCT.2017.11.052

24. Zhuo P, Li S, Ashcroft IA, Jones AI (2021) Material extrusion additive manufacturing of continuous fibre reinforced polymer matrix composites: a review and outlook. Compos B Eng 224:109143. https://doi.org/10.1016/J.COMPOSITESB.2021.109143

25. Rimašauskas M, Jasiūnienė E, Kuncius T, Rimašauskienė R, Cicėnas V (2022) Investigation of influence of printing parameters on the quality of 3D printed composite structures. Compos Struct 281:115061. https://doi.org/10.1016/J.COMPSTRUCT.2021.115061

26. Papon EA, Haque A (2018) Tensile properties, void contents, dispersion and fracture behaviour of 3D printed carbon nanofiber reinforced composites. J Reinf Plast Compos 37:381–395. https://doi.org/10.1177/0731684417750477

27. Jang S, Boddorff A, Jang DJ, Lloyd J, Wagner K, Thadhani N, Brettmann B (2021) Effect of material extrusion process parameters on filament geometry and inter-filament voids in as-fabricated high solids loaded polymer composites. Addit Manuf 47:102313. https://doi.org/10.1016/J.ADDMA.2021.102313

28. Hu Q, Duan Y, Zhang H, Liu D, Yan B, Peng F (2018) Manufacturing and 3D printing of continuous carbon fiber prepreg filament. J Mater Sci 53:1887–1898. https://doi.org/10.1007/S10853-017-1624-2/FIGURES/10

29. Chacón JM, Caminero MA, Núñez PJ, García-Plaza E, García-Moreno I, Reverte JM (2019) Additive manufacturing of continuous fibre reinforced thermoplastic composites using fused deposition modelling: effect of process parameters on mechanical properties. Compos Sci Technol 181:107688. https://doi.org/10.1016/J.COMPSCITECH.2019.107688

30. Blok LG, Longana ML, Yu H, Woods BKS (2018) An investigation into 3D printing of fibre reinforced thermoplastic composites. Addit Manuf 22:176–186. https://doi.org/10.1016/J.ADDMA.2018.04.039

31. Azlin MNM, Sapuan SM, Zuhri MYM, Zainudin ES (2022) Effect of stacking sequence and fiber content on mechanical and morphological properties of woven kenaf/polyester fiber reinforced polylactic acid (PLA) hybrid laminated composites. J Market Res 16:1190–1201. https://doi.org/10.1016/J.JMRT.2021.12.046

32. Shi K, Yan Y, Mei H, Chen C, Cheng L (2021) 3D printing Kevlar fiber layer distributions and fiber orientations into nylon composites to achieve designable mechanical strength. Addit Manuf 39:101882. https://doi.org/10.1016/J.ADDMA.2021.101882

33. Wang K, Long H, Chen Y, Baniassadi M, Rao Y, Peng Y (2021) Heat-treatment effects on dimensional stability and mechanical properties of 3D printed continuous carbon fiber-reinforced composites. Compos Part A Appl Sci Manuf 147:106460. https://doi.org/10.1016/J.COMPOSITESA.2021.106460

34. Caminero MA, Chacón JM, García-Moreno I, Reverte JM (2018) Interlaminar bonding performance of 3D printed continuous fibre reinforced thermoplastic composites using fused deposition modelling. Polym Test 68:415–423. https://doi.org/10.1016/J.POLYMERTESTING.2018.04.038

35. Standard test method for through-thickness "flatwise" tensile strength and elastic modulus of a fiber-reinforced polymer matrix composite material, (n.d.). https://www.astm.org/d7291_d7291m-15.html

36. Standard test method for compressive properties of rigid plastics, (n.d.). https://www.astm.org/d0695-15.html

37. Standard test method for short-beam strength of polymer matrix composite materials and their laminates, (n.d.). https://www.astm.org/d2344_d2344m-16.html

38. Wang G, Zhang D, Li B, Wan G, Zhao G, Zhang A (2019) Strong and thermal-resistance glass fiber-reinforced polylactic acid (PLA) composites enabled by heat treatment. Int J Biol Macromol 129:448–459. https://doi.org/10.1016/J.IJBIOMAC.2019.02.020

39. Bhandari S, Lopez-Anido RA, Gardner DJ (2019) Enhancing the interlayer tensile strength of 3D printed short carbon fiber reinforced PETG and PLA composites via annealing. Addit Manuf 30:100922. https://doi.org/10.1016/J.ADDMA.2019.100922

40. Markforged (2021) Material datasheet: composites. https://static.markforged.com/downloads/composites-data-sheet.pdf

41. Pascual-González C, San Martín P, Lizarralde I, Fernández A, León A, Lopes CS, Fernández-Blázquez JP (2021) Post-processing effects on microstructure, interlaminar and thermal properties of 3D printed continuous carbon fibre composites. Compos B Eng 210:108652. https://doi.org/10.1016/J.COMPOSITESB.2021.108652

42. Parmiggiani A, Prato M, Pizzorni M (2021) Effect of the fiber orientation on the tensile and flexural behavior of continuous carbon fiber composites made via fused filament fabrication. The International Journal of Advanced Manufacturing Technology 114:2085–2101. https://doi.org/10.1007/s00170-021-06997-5

43. Kim BC, Park DC, Kim BJ, Lee DG (2010) Through-thickness compressive strength of a carbon/epoxy composite laminate.

Compos Struct 92:480–487. https://doi.org/10.1016/J.COMPS TRUCT.2009.08.032

44. San Juan V, Fernández E, Pincheira G, Meléndrez M, Flores P (2016) Evaluation of the fill yarns effect on the out-of-plane compressive fatigue behavior for an unidirectional glass fiber reinforced epoxy composite. Compos Struct 138:237–242. https://doi.org/10.1016/J.COMPSTRUCT.2015.11.061

45. Hart KR, Dunn RM, Wetzel ED (2020) Increased fracture toughness of additively manufactured semi-crystalline thermoplastics via thermal annealing. Polymer (Guildf) 211:123091. https://doi.org/10.1016/J.POLYMER.2020.123091

46 Hart KR, Dunn RM, Sietins JM, C.M. (2018) Hofmeister Mock, M.E. Mackay, E.D. Wetzel, Increased fracture toughness of additively manufactured amorphous thermoplastics via thermal annealing. Polymer (Guildf) 144:192–204. https://doi.org/10.1016/J.POLYMER.2018.04.024